GEOPHYSICS, VOL. 86, NO. 3 (MAY-JUNE 2021); P. U31–U37, 6 FIGS., 3 TABLES.
10.1190/GEO2020-0117.1

Acoustic properties of hydrate-bearing coal samples depending on temperature and water saturation type

Geser A. Dugarov[1], Anton A. Duchkov[2], and Andrey Yu. Manakov[3]

ABSTRACT

We have developed the first experimental acoustic properties measurement during gas-hydrate formation and dissociation in crushed bituminous coal samples. We also compare the results with acoustic properties measurements during freezing and thawing water in the same samples. The results show a more complicated behavior that differs from similar experiments with sand. For the samples with adsorbed water, it does not freeze at anticipated temperatures, but acoustic velocities gradually increase with the decreasing negative temperatures. It is caused by complicated pore surface structures causing partial formation of ice/hydrate from bound water at different temperatures. We also observe that, for the same samples, the acoustic properties change significantly, becoming stronger during gas-hydrate formation than during freezing. We explain it by competitive sorption of methane and water in the coal pore space; methane under pressure replaces part of the adsorbed water from micropores so that this water can easily form hydrate. The difference in the acoustic properties of frozen and hydrate-bearing coal samples is important for developing seismic methods for geophysical characterization of coal seams.

INTRODUCTION

Natural gas hydrates are formed at high pressure and low temperature in the presence of free water and a hydrate-forming gas (e.g., methane). Suitable pressures and temperatures exist within the hydrate stability zone, which is widespread in oceanic sediments and permafrost regions. Usually, natural gas-hydrate accumulations appear close to the sources of natural gas. Makogon (1974) first introduces the idea that gas hydrates may form in coal bodies because water and methane are usually abundant there due to coal metamorphism. In particular, Smirnov et al. (2016, 2018) argue that several coal basins have thermobaric conditions suitable for gas-hydrate formation. This is especially true for coal basins in northern regions where the hydrate stability zone usually has a thickness of 100–800 m starting from the depth of 250 m (Collett, 2002). In particular, the Pechora Basin is located in the permafrost region and its gas component is a mixture of methane and heavy hydrocarbons, which can form hydrate at a lower pressure or a higher temperature than pure methane.

Laboratory studies confirmed the possibility of hydrate formation from water in natural coals (Bustin et al., 2016; Smirnov et al., 2016, 2018). But the physical properties of hydrate-bearing coal samples have not been studied yet. Previously, we used a specialized laboratory setup to form methane gas-hydrates in sand samples and to study their acoustic properties (Duchkov et al., 2018, 2019; Dugarov et al., 2019). Specialized laboratory setups are commonly used to form gas hydrates in rock samples (Winters et al., 2000; Kulenkampff and Spangenberg, 2005; Priegnitz et al., 2013). They allow studying physical properties of hydrate-bearing samples depending on various factors including the rock-matrix material, type of pore fluid, and the amount and morphology of hydrate in pores. The rock-matrix material and gas-hydrate morphology (how hydrate interacts with sediment grain) appear to be dominant factors determining the resultant acoustic macroproperties. For sand samples, different morphologies of hydrate in the pore space are mostly the result of different scenarios of hydrate formation (Priest et al., 2009; Waite et al., 2009; Dugarov et al., 2019), but coal, unlike sand, has a complex multiscale porosity structure (Cai et al., 2018; Pan et al., 2019).

Coal commonly contains matrix, clay minerals, numerous pores, and small fractures. The size of pores and fractures ranges from nm

Manuscript received by the Editor 25 February 2020; revised manuscript received 11 November 2020; published ahead of production 9 January 2021; published online 11 March 2021.
[1]Trofimuk Institute of Petroleum Geology and Geophysics SB RAS, Novosibirsk 630090, Russia. E-mail: dugarovga@ipgg.sbras.ru (corresponding author).
[2]Trofimuk Institute of Petroleum Geology and Geophysics SB RAS, Novosibirsk, Russia and Novosibirsk State University, Novosibirsk 630090, Russia. E-mail: duchkovaa@ipgg.sbras.ru.
[3]Novosibirsk State University, Novosibirsk, Russia and Nikolaev Institute of Inorganic Chemistry SB RAS, Novosibirsk 630090, Russia. E-mail: manakov@niic.nsc.ru.

DOI:10.1190/geo2020-0117.1

to mm scale. Because of the porous nature and diverse chemical decoration of the surface, coal is an excellent sorbent, which should have a prevailing influence on the morphology of gas-hydrate formation. In this work, we formed methane gas-hydrates in samples from natural bituminous coal and presented the first experimental acoustic property measurement during hydrate formation and dissociation in samples with different initial water saturations.

METHODS

Samples preparation

Coal for the samples was taken from an operating mine of the Kuznetsk coal basin in Russia (the Kemerovo region). We used low-volatility bituminous coal from bed XXIV of the Pervomayskaya coalmine, which is an outburst mine (Jones, 2005). The results of the technical analysis of this coal are presented in Table 1. The density of the coal frame is 1.31 g/cm^3 as measured by the pycnometric method. The original porosity of the coal was 0.18 as measured by the mercury intrusion test.

For acoustic experiments, we wanted to guarantee homogeneous samples with homogeneous water saturation. Accordingly, we first crushed the coal into a powder with a particle size between 0.2 and 1 mm. Then, we saturated the coal powder with water and put it into a Caprolon cell. Finally, we compacted this sample with a hydraulic press (at 10 MPa). The resultant sample was 26 mm in diameter and 40–50 mm long. The effective density of the samples varies from 1.1 to 1.2 g/cm^3.

We used three types of water saturation: dry coal, coal with only adsorbed water, and coal with adsorbed and free water in pores, because of the complex multiscale porosity structure. For this, we first dried the coal material at 110°C under vacuum conditions. Then, for some samples we added adsorbed water by placing coal into a desiccator with water at the bottom. Finally, for some samples we added water so that they contained adsorbed and capillary water, which we will further call free water. Only distilled water was used in the experiments.

Further, we will discuss experimental results of studying acoustic properties of three samples. The samples differ only by the type of water saturation; see Table 2. The experimental procedure was the same for each sample.

Table 1. Results of the technical analysis of the coal from the Pervomayskaya coal mine: A_d, ash content on a dry basis; V_{daf}, volatile compounds content on a dry ash-free basis; and C_{daf} and H_{daf}, carbon and hydrogen content, respectively, on a dry ash-free basis.

A_d (%)	V_{daf} (%)	C_{daf} (%)	H_{daf} (%)	Functional group concentration, mg–eq/g (daf)		
				COOH	CO	COOH + OH
5.1	20.5	89.66	5.08	< 0.01	0.101	0.036

Table 2. Parameters of the coal samples. All mass values are given for 100 g of dry coal: S_h, hydrate saturation after finishing the hydrate formation (the volume fraction of the pore space occupied by hydrate); $M_{w,trans}$, the mass of water transformed to hydrate; $M_{w,free}$, the mass of free water; and $M_{w,ads}$, the mass of adsorbed water.

Sample ID	Water state	S_h	Porosity	$M_{w,trans}$, g	$M_{w,free}$, g	$M_{w,ads}$, g
Cdry	No	0	0.15	0	0	0
Cads	Adsorbed	0.18	0.13	1.7	0	2.7
Cboth	Adsorbed and free	0.59	0.11	3.6	3.3	2.7

Experimental procedure

The cell with the sample was loaded into a high-pressure chamber (Figure 1). Two plungers with piezoceramic acoustic sensors were attached to the top and the bottom of the sample under axial pressure; see Duchkov et al. (2017) for details. Constant axial and lateral pressure of 30 MPa was maintained during the experiments. We could vary the pore pressure and temperature in the chamber with time while measuring the acoustic properties every 5 min: the velocities of the compressional (P) and shear (S) waves in the sample.

We first froze all of the samples and measured the acoustic properties of the coal with ice. Then, we injected methane into the pores of the sample at an initial pressure of 10 MPa. We performed experiments of hydrate formation under the "excess-gas" condition. After methane injection, we increased the temperature to the values outside the methane-hydrate stability zone and kept it constant for approximately 24 h. Methane adsorption was taking place during this period, which was indicated by the slow pore-pressure decrease.

For initiation of the hydrate formation, we lowered the temperature so that methane gas hydrate may form; see stage A-B in Figure 2. During the stage of hydrate formation (stage B-C), we observed a gas pressure decrease due to the combined impact of hydrate formation, methane adsorption by coal, and possible small leakages from the gas line. In some cases, we used temperature cycles (going from negative to positive temperatures without going above the methane hydrate phase boundary) to speed up the hydrate formation due to freezing-thawing of the remaining water (Chuvilin

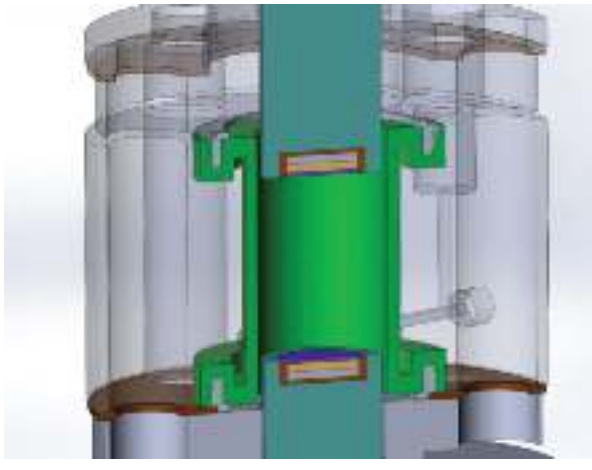

Figure 1. Schematic view of the high-pressure chamber consisting of a steel vessel (gray), rubber collar maintaining lateral pressure (green), and two plungers maintaining axial pressure (mint) with piezoceramic acoustic sensors.

DOI:10.1190/geo2020-0117.1

and Guryeva, 2009; Li et al., 2011). The changes of the P- and S-wave velocities in time during hydrate formation (and water freezing) were similar to the case of using sand samples (Duchkov et al., 2019; Dugarov et al., 2019).

In the case of water, the freezing velocities stayed constant (see Figure 3a), but it should be mentioned that time-limited data are available for this case (approximately 3 h). In the case of hydrate formation, we observed slow velocities increase (within a 3 h interval), which continued for 10–20 days, see Figure 3b. The increasing velocities indicated the increasing amount of methane hydrate in the sample. Stabilization of the P- and S-wave velocities at high values during temperature cycles is an indicator that the maximum gas-hydrate formation is complete. A distinctive feature of the experiments with coal was their duration as compared to similar experiments with sand (approximately five times faster).

After finishing the hydrate formation, we studied acoustic properties of hydrate-bearing samples at different temperatures. For this, we froze samples, stage C-D in Figure 2, and slowly increased the temperature from a negative value to the value above the methane hydrate phase boundary, stage D-E in Figure 2. Changes in the P-wave velocity during stages C-D and D-E are shown in Figure 4a. The temperature increase rate was 0.5°C per hour as shown by the green line in the figure (the right axis). In Figure 4a, one can clearly see the P-wave velocity variations due to the changes in temperature. One can rearrange these data showing the dependence of acoustic velocities on the sample temperature; see Figure 4b. The blue curve for the interval from −10°C to +11°C shows the clear dependence of the P-wave velocity from the sample temperature.

The final experiment stage included hydrate dissociation as one can see in Figure 4a (interval 295–300 h) and Figure 4b (interval 11°C–15°C). The hydrate dissociation results in the release of methane gas, which leads to quick pore-pressure increase and acoustic velocity drop (Figure 4b). For each experiment, we used this quick pore-pressure increase estimating the gas volume released during hydrate dissociation, which then was used for estimation of the final hydrate saturation (the volume fraction of the pore space occupied by the hydrate) in the sample. Thus, we can obtain data from one experiment about acoustic properties at only one hydrate saturation.

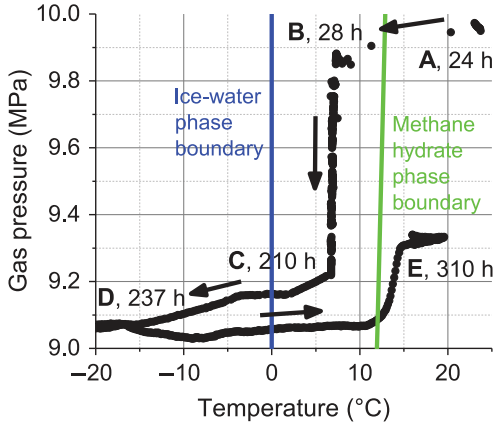

Figure 2. Changes of gas pressure versus temperature during: (A-B) temperature lowering for the initiation of hydrate formation, (B-C) methane hydrate formation, (C-D) sample freezing, and (D-E) temperature raising with hydrate dissociation in the end. The colored lines are phase boundaries of ice-water (blue) and methane hydrate (green).

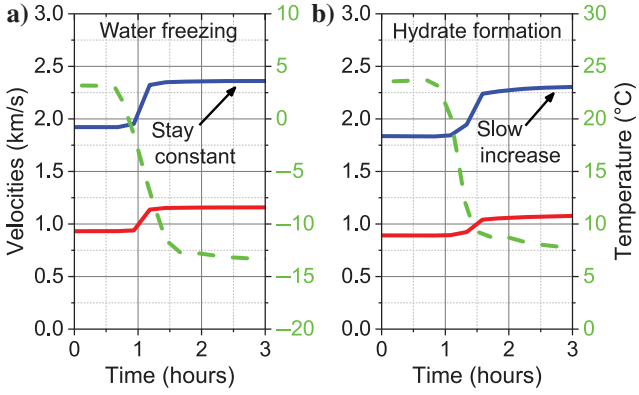

Figure 3. The changes in the P- (the blue lines) and S-wave (the red lines) velocities during (a) water freezing and (b) hydrate formation with temperature decrease (the green line).

RESULTS AND DISCUSSION

Here, we present experimental results for three coal samples with different types of water saturation: dry coal (Cdry), coal with only adsorbed water (Cads), and coal with adsorbed and free water (Cboth); see Table 2. The samples were made of pressed fractionated coal. For this reason, the measured velocities were lower than the velocities in undeformed coal (Morcote et al., 2010; Chen et al., 2017).

The initial acoustic properties of the samples are within the range of 1.6–2.0 km/s for the P-wave and 0.85–0.95 km/s for the S-wave. These values are slightly lower than the acoustic properties of undeformed coal (Morcote et al., 2010; Chen et al., 2017). They appear to be similar to samples from the shear and plastic deformation environment in Chen et al. (2017) and higher than the properties of the powder samples in Morcote et al. (2010). Note that the ratio of the

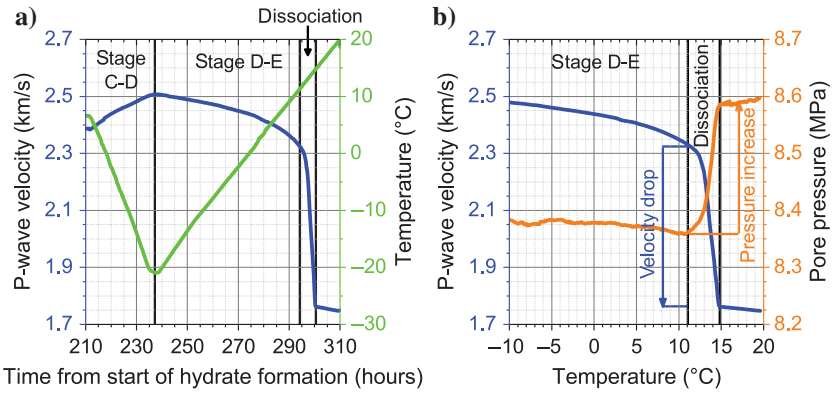

Figure 4. Example of experimental data representations: (a) variations in P-wave velocity (the blue line) during temperature variations (the green line) and (b) dependence of P-wave velocity from the temperature (the blue line) and pore pressure in the sample (the orange line).

P- to S-wave velocity is < 1.9 for the dry sample and the sample with adsorbed water; for the sample with adsorbed and free water, this ratio is ≥2.0.

From Table 2, we see that not all of the water is transformed into the hydrate form. The mass of water transformed to hydrate is less than the total mass of free and adsorbed water. For both samples containing water (Cads and Cboth), only approximately 60% of the water is transformed into the hydrate form despite the very long duration of the experiment — more than 10 days. We explain it by the presence of considerable amounts of the adsorbed water trapped in tiny pores of coal. This is different from the sand samples containing mostly free water surrounding grains (in the case of using the excess-gas method). In sand samples, almost all of the water transforms into the hydrate form in a couple of days (Duchkov et al., 2017). For the coal samples containing water (Cads and Cboth), we see that the mass of free water is less than the mass of water transformed to hydrate (Table 2). Thus, we assume that almost all of the free water in the sample Cboth was transformed into the hydrate. But we also see that part of the adsorbed water was also transformed into the hydrate.

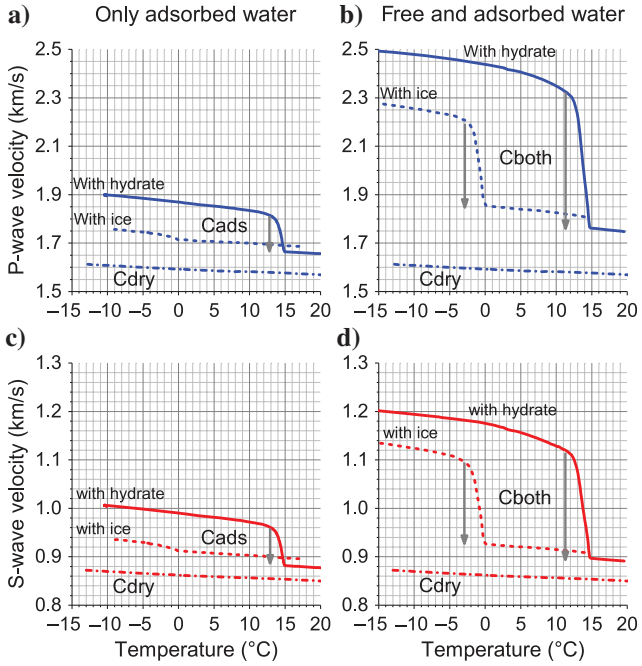

Figure 5. The changes in (a and b) P- and (c and d) S-wave velocities with the temperature increase for the samples made of dry coal (the dashed-dotted lines): (a and c) coal containing only adsorbed water, (b and d) coal containing adsorbed and free water during phase transitions — ice melting (the dashed lines) or methane hydrate dissociation (the solid lines). Velocity drops are marked by gray arrows.

For better insight into the behavior of the adsorbed water, we show changes in the acoustic velocities with temperature in Figure 5 for all samples from Table 2 (Cdry, Cads, and Cboth). The representation of the results is similar to Figure 4b. The P-wave velocities are shown in blue (Figure 5a and 5b), the S-wave velocities are in red (Figure 5c and 5d). In all panels, we show the acoustic velocities for the dry sample (Cdry) by a dashed-dotted line. For Cdry, we see a constant descending trend (−1.5 m/s/°C) — the acoustic velocities decrease with the increasing temperature. In the left column, we add the acoustic properties for the sample with only adsorbed water (Cads); in the right column — for the sample with adsorbed and free water (Cboth). For both cases, we first freeze/thaw the samples (pore pressure of 0.1 MPa, no methane) as shown by the dashed lines. Then, we form and decompose the gas hydrates (methane in pores at pressure of approximately 10 MPa) as shown by the solid lines. In the temperature range corresponding to the stability of hydrate or ice, a gradual decrease in the velocities is observed, accelerating as the phase transition temperature approaches. We expect to see velocity drops at the phase transition temperatures: 0°C for thawing, approximately 13°C for the hydrate dissociation. An estimate of the velocity change during phase transitions — ice melting or methane hydrate dissociation — is shown in Table 3. First, we will discuss the differences in the velocity drops, and then the continuous trend of the velocity decreases with the increasing temperatures.

The most interesting results concerning the velocity drop were obtained for the Cads sample containing only adsorbed water. Note that there is no sharp freezing/thawing increase in velocities for the sample with adsorbed water; see the dashed lines in Figure 5a and 5c. There is no visible velocity drop at the formal temperature of the phase transition, that is, 0°C. This corresponds to the available literature data, according to which all of the water in such samples (with adsorbed water) is in thin pores and does not show freeze-thaw phase transitions at a certain temperature (Charrière and Behra, 2010; Smirnov et al., 2016, 2018). There is also some difference in the slope of the temperature dependence for negative and positive temperatures that we will discuss in more detail later in this section.

But for the hydrate dissociation in the sample Cads, we clearly see the velocity drops due to the hydrate dissociation (the solid lines in Figure 5a and 5c): 0.18 km/s (10%) and 0.09 km/s (10%) for the P- and S-waves, respectively. We relate this phenomenon to the change of the water state in the coal sample. It can be explained by the

Table 3. Velocity drop for the P- and S-waves during phase transitions — ice melting or methane hydrate dissociation. The ΔV_P and ΔV_S for samples with ice are the differences in the P- and S-wave velocities at temperatures –5 and 5°C, for samples with methane hydrate — at temperatures 10°C and 20°C.

Sample ID	Phase transition	ΔV_P (km/s)	ΔV_S (km/s)	ΔV_P (%)	ΔV_S (%)
Dry coal					
Cdry	No	—	—	—	—
Adsorbed water					
Cads	Ice — water	—	—	—	—
Cads	Hydrate — water + gas	0.18	0.09	10	10
Adsorbed and free water					
Cboth	Ice — water	0.39	0.19	19	19
Cboth	Hydrate — water + gas	0.60	0.24	29	24

competitive sorption of methane and water in the coal pores (Ceglarska-Stefańska and Zarębska, 2002; Merkel et al., 2015; Zeng et al., 2017; Smirnov et al., 2018, 2020). The model proposed by Smirnov et al. (2020) supposes water displacement from thin pores by the adsorbed gas and hydrate formation from this water. Part of the weakly bound water localized in the form of microdrops on sufficiently hydrophilic regions of the surface of coal micropores is displaced by methane into the pore space between coal grains due to the effect of competitive sorption. This water then behaves like free water: it forms hydrate easier affecting acoustic properties more, similarly to hydrate formation in sand samples. This effect could explain the drastic difference between the behavior of the acoustic properties in the experiments with freezing and hydrate formation.

For the Cboth sample containing adsorbed and free water, we observe the velocity drop in both types of experiments; see Figure 5b and 5d. But these velocity drops are smaller for ice melting — 0.39 km/s (19%) for the P-wave and 0.19 km/s (19%) for the S-wave; and larger for the hydrate formation — 0.60 km/s (29%) and 0.24 km/s (24%). Note that in sand we do not see considerable differences in the acoustic properties between freezing or hydrate formation in the same sample. Thus, we conclude that in the case with coal samples some of the adsorbed water is removed from micropores as well. We suggest that the process of competitive sorption also takes place in the case in which some free water is already present in the sample pore space.

In the preceding discussion, we have discussed the velocity decreases that happen around temperatures of the phase transition (ice and hydrate formation/dissociation). For the curves in Figure 5, we also see that a descending trend of acoustic properties decreases with the increasing temperature. For the dry sample (Cdry), the slope is constant for the negative and positive temperatures at approximately −1.5 m/s/°C. We will ignore this linear trend because it could be caused (at least in part) by small deformations in the laboratory setup at different temperatures. However, we see that the dependence of acoustic properties on temperature becomes stronger for the sample with adsorbed water (Cabs); see the dashed lines in Figure 5a and 5c. There is no visible velocity drop at 0°C, but apparently the adsorbed water causes some additional hardening of the sample with the decreasing negative temperature. One can see a similar hardening trend for other samples in the case of ice and hydrate formation. Considering the linear part at negative temperatures, the linear trend is approximately −3 m/s/°C to −4.5 m/s/°C.

This consistent decrease of the acoustic velocities in the sample with the increasing temperature can be explained using the existing model of moisture freezing and hydrate formation in rocks (Chuvilin et al., 2011). Due to the interaction with the surface of the rock particles, the water in the rock has a spectrum of energy states. Bound water freezes (or forms a hydrate) at a lower temperature than bulk water. With the decreasing temperature, more and more water is transformed into ice/hydrate (Dash et al., 1995). But the most strongly bound part of the water may not freeze at all or may not transform to hydrate. For experiments with sand, Chaouachi et al. (2015), Sell et al. (2016), Yang et al. (2016), and Sahoo et al. (2018) use high-resolution X-ray computed tomography imaging to study the microstructure of hydrate in the pore space. Sahoo et al. (2018) form methane gas hydrate, whereas Chaouachi et al. (2015), Sell et al. (2016), and Yang et al. (2016) form xenon gas hydrate. But all authors claim that a thin water film remains between the sand particles and the gas hydrate. This can be a rough analogy to what is taking place in our coal samples for which there is no high-resolution tomography imaging available.

The surface of the coal used in our experiments (Smirnov et al., 2020) contains polar functional groups; see Table 1. In addition, the coal contains ash, which is a complex mixture of minerals with a complicated surface geometry. Such complex surfaces can bind significant quantities of water. At a given pressure, the freezing (or hydrate formation) of such water is taking place within the range of temperatures. This leads to a gradual formation/dissociation of ice or hydrate at decreasing/increasing temperatures. We assume that the decrease of the velocities observed with the temperature increasing is associated with the partial dissociation of the hydrate in the sample leading to the weakening of the bonds between the coal particles.

We also performed a similar set of experiments for the same type of coal from another coal mine: low-volatile bituminous coal from bed XXVII of the Berezovskaya coal mine, the Kemerovo region of the Kuznetsk coal basin. In the experiments with this coal, we also observed similar features as discussed above: the velocity decreases that we associate with the competitive sorption of methane replacing adsorbed water and the temperature dependence of the acoustic velocities. The obtained P- and S-wave velocities on this set of samples in comparison with the previously discussed samples from the Pervomayskaya coal mine are shown in Figure 6. Note that the porosity of the sample set from the Berezovskaya coal mine was 0.21 and we used a higher initial gas pressure of 15 MPa. Despite this fact, the estimated velocities in the samples formed from coal from different coal mines are in good accordance. The acoustic P- and S-wave velocities increase modestly for the studied range of hydrate saturation (less than 0.6).

Velocities estimated from contact-cementing, envelope-cementing, and load-bearing (noncementing) effective models for describing acoustic properties of hydrate-bearing samples (Dvorkin and Nur, 1996; Ecker et al., 1998) are also shown in Figure 6. We can conclude that the load-bearing model is better for fitting experimental P- and S-wave velocity values for coal samples with methane gas hydrates. This result differs from the result for methane-hydrate-

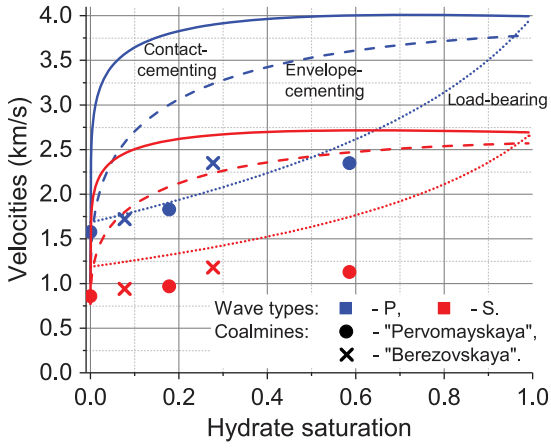

Figure 6. The P- and S-wave velocities (at 10°C) in samples formed from coal from the Pervomayskaya (the circles) and Berezovskaya (the crosses) coal mines in comparison with estimation by contact-cementing (the solid lines), envelope-cementing (the dashed lines), and load-bearing (the dotted lines) effective models.

bearing sand samples (Dugarov et al., 2019), as expected. In the case of sand samples, the envelope-cementing model is the best for fitting the velocity values. However, more experiments on methane gas-hydrate formation in coal samples are needed for more detailed analysis of velocity dependencies from hydrate saturation.

CONCLUSION

In this paper, we have demonstrated the results of experiments on studying acoustic properties (P- and S-wave velocities) of samples from low-volatile bituminous coal during freezing and methane-hydrate formation. Typically, for sand samples we see a rapid velocity drop during ice/hydrate dissociation. For coal samples, this effect strongly depends on the type of initial water saturation. For the samples with free water, we observed a clear velocity increase/decrease similar to experiments with sand. For the samples with only adsorbed water, there is no velocity change during freezing/thawing. There is also a continuous trend of hardening (velocity increase) with decreasing negative temperatures. We interpret these results as a manifestation of the complicated pore structure of coal. A complex geometry of coal pore surfaces significantly changes the energy state of bound water, leading to a partial formation of ice/hydrate at different temperatures.

Another experimental observation is that, for the same samples, changes in acoustic properties were significantly stronger during gas-hydrate formation than during freezing. For the sample with only adsorbed water, there was no velocity change during freezing/thawing but there was a noticeable velocity increase/decrease during the hydrate formation/dissociation. This result is different from experiments with sand where freezing or hydrate formation results in a very similar increase of acoustic velocities. A possible explanation of this effect in the coal samples could be that the presence of methane under pressure in the pore space results in replacing part of the adsorbed water from the micropores. This replaced water starts behaving like free water easily forming hydrate, causing changes in the acoustic properties. Thus, we interpret these results as an experimental confirmation of the competitive sorption of methane and water in thin coal pores.

From a geophysical point of view, the presented results are significant because they show different acoustic properties for the same sample containing ice or hydrate (note that in most cases frozen and hydrate-bearing samples show similar physical properties). This paves the way to develop seismic methods for coal seam characterization and monitoring. To better understand the addressed processes, we need high-resolution tomographic imaging of the hydrate formation in coal samples. This will give hard evidence for supporting our interpretation of the variation in acoustic properties.

ACKNOWLEDGMENTS

We are grateful to V.G. Smirnov for providing the coal samples. The work was supported by the Russian Science Foundation (grant no. 19-77-00068).

DATA AND MATERIALS AVAILABILITY

Data associated with this research are available and can be obtained by contacting the corresponding author.

REFERENCES

Bustin, A. M. M., R. M. Bustin, I. L. Moudrakovskim, S. Takeya, and J. A. Ripmeester, 2016, Formation of methane clathrate hydrates in coal moisture: Implications for coalbed methane resources and reservoir pressures: Energy & Fuels, **30**, 88–97, doi: 10.1021/acs.energyfuels.5b01922.

Cai, T. T., Z. C. Feng, and D. Zhou, 2018, Multi-scale characteristics of coal structure by X-ray computed tomography (X-ray CT), scanning electron microscope (SEM) and mercury intrusion porosimetry (MIP): AIP Advances, **8**, 025324, doi: 10.1063/1.5021699.

Ceglarska-Stefańska, G., and K. Zarębska, 2002, The competitive sorption of CO2 and CH4 with regard to the release of methane from coal: Fuel Processing Technology, **77-78**, 423–429, doi: 10.1016/S0378-3820(02)00093-0.

Chaouachi, M., A. Falenty, K. Sell, F. Enzmann, M. Kersten, D. Haberthür, and W. F. Kuhs, 2015, Microstructural evolution of gas hydrates in sedimentary matrices observed with synchrotron X-ray computed tomographic microscopy: Geochemistry, Geophysics, Geosystems, **16**, 1711–1722, doi: 10.1002/2015GC005811.

Charrière, D., and P. Behra, 2010, Water sorption on coals: Journal of Colloid and Interface Science, **344**, 460–467, doi: 10.1016/j.jcis.2009.11.064.

Chen, H., B. Jiang, T. Chen, S. Xu, and G. Zhu, 2017, Experimental study on ultrasonic velocity and anisotropy of tectonically deformed coal: International Journal of Coal Geology, **179**, 242–252, doi: 10.1016/j.coal.2017.06.003.

Chuvilin, E. M., and O. M. Guryeva, 2009, Experimental investigation of CO2 gas hydrate formation in porous media of frozen and freezing sediments: Earth's Cryosphere, **13**, 70–79.

Chuvilin, E. M., V. A. Istomin, and S. S. Safonov, 2011, Residual nonclathrated water in sediments in equilibrium with gas hydrate: Comparison with unfrozen water: Cold Regions Science and Technology, **68**, 68–73, doi: 10.1016/j.coldregions.2011.05.006.

Collett, T. S., 2002, Energy resource potential of natural gas hydrates: AAPG Bulletin, **86**, 1971–1992, doi: 10.1306/61EEDDD2-173E-11D7-8645000102C1865D.

Dash, J. G., H. Fu, and J. S. Wettlaufer, 1995, The premelting of ice and its environmental consequences: Reports on Progress in Physics, **58**, 115–167, doi: 10.1088/0034-4885/58/1/003.

Duchkov, A. D., A. A. Duchkov, G. A. Dugarov, and A. N. Drobchik, 2018, Velocities of ultrasonic waves in sand samples containing water, ice, or methane and tetrahydrofuran hydrates (laboratory measurements): Doklady Earth Sciences, **478**, 74–78, doi: 10.1134/S1028334X18010014.

Duchkov, A. D., A. A. Duchkov, M. E. Permyakov, A. Y. Manakov, N. A. Golikov, and A. N. Drobchik, 2017, Acoustic properties of hydrate-bearing sand samples: Laboratory measurements (setup, methods, and results): Russian Geology and Geophysics, **58**, 727–737, doi: 10.1016/j.rgg.2016.09.029.

Duchkov, A. D., G. A. Dugarov, A. A. Duchkov, and A. N. Drobchik, 2019, Laboratory investigations into the velocities and attenuation of ultrasonic waves in sand samples containing water/ice and methane and tetrahydrofuran hydrates: Russian Geology and Geophysics, **60**, 193–203, doi: 10.15372/RGG2019015.

Dugarov, G. A., A. A. Duchkov, A. D. Duchkov, and A. N. Drobchik, 2019, Laboratory validation of effective acoustic velocity models for samples bearing hydrates of different type: Journal of Natural Gas Science and Engineering, **63**, 38–46, doi: 10.1016/j.jngse.2019.01.007.

Dvorkin, J., and A. Nur, 1996, Elasticity of high-porosity sandstones: Theory for two North Sea data sets: Geophysics, **61**, 1363–1370, doi: 10.1190/1.1444059.

Ecker, C., J. Dvorkin, and A. Nur, 1998, Sediments with gas hydrates: Internal structures from seismic AVO: Geophysics, **63**, 1659–1669, doi: 10.1190/1.1444462.

Jones, N. S., 2005, A review of the AMM & CMM resources in the Kuznetsk (Kuzbass) Coal Basin, Russia: British Geological Survey Internal Report, IR/05/135.

Kulenkampff, J., and E. Spangenberg, 2005, Physical properties of cores from the Mallik 5L-38 gas hydrate production research well under simulated in situ conditions using the Field Laboratory Experimental Core Analysis System (FLECAS), *in* S. R. Dallimore and T. S. Collett, eds., Scientific Results from the Mallik 2002 gas hydrate production research well program, Mackenzie Delta, Northwest Territories, Canada: Geological Survey of Canada, GSC Bulletin **585**.

Li, D., D. Wang, and D. Liang, 2011, P-wave of hydrate-bearing sand under temperature cycling: Geophysics, **76**, no. 1, E1–E7, doi: 10.1190/1.3515263.

Makogon, Y. F., 1974, Hydrates of natural gases [in Russian]: Nedra.

Merkel, A., Y. Gensterblum, B. M. Krooss, and A. Amann, 2015, Competitive sorption of CH4, CO2 and H2O on natural coals of different rank: International Journal of Coal Geology, **150-151**, 181–192, doi: 10.1016/j.coal.2015.09.006.

Morcote, A., G. Mavko, and M. Prasad, 2010, Dynamic elastic properties of coal: Geophysics, **75**, no. 6, E227–E234, doi: 10.1190/1.3508874.
Pan, J., Z. Zhang, M. Li, Y. Wu, and K. Wang, 2019, Characteristics of multi-scale pore structure of coal and its influence on permeability: Natural Gas Industry B, **6**, 357–365, doi: 10.1016/j.ngib.2019.01.012.
Priegnitz, M., J. Thaler, E. Spangenberg, C. Rücker, and J. M. Schicks, 2013, A cylindrical electrical resistivity tomography array for three dimensional monitoring of hydrate formation and dissociation: Review of Scientific Instruments, **84**, 104502, doi: 10.1063/1.4825372.
Priest, J. A., E. V. L. Rees, and C. R. I. Clayton, 2009, Influence of gas hydrate morphology on the seismic velocities of sands: Journal of Geophysical Research, **114**, B11205, doi: 10.1029/2009JB006284.
Sahoo, S. K., B. N. Madhusudhan, H. Marín-Moreno, L. J. North, S. Ahmed, I. H. Falcon-Suarez, T. A. Minshull, and A. I. Best, 2018, Laboratory insights into the effect of sediment-hosted methane hydrate morphology on elastic wave velocity from time-lapse 4-D synchrotron X-ray computed tomography: Geochemistry, Geophysics, Geosystems, **19**, 4502–4521, doi: 10.1029/2018GC007710.
Sell, K., E. H. Saenger, A. Falenty, M. Chaouachi, D. Haberthür, F. Enzmann, W. F. Kuhs, and M. Kersten, 2016, On the path to the digital rock physics of gas hydrate-bearing sediments – processing of in situ synchrotron-tomography data: Solid Earth, **7**, 1243–1258, doi: 10.5194/se-7-1243-2016.
Smirnov, V. G., V. V. Dyrdin, A. Y. Manakov, and Z. R. Ismagilov, 2020, Decomposition of carbon dioxide hydrate in the samples of natural coal with different degrees of metamorphism: Chinese Journal of Chemical Engineering, **28**, 492–501, doi: 10.1016/j.cjche.2019.06.002.
Smirnov, V. G., A. Y. Manakov, V. V. Dyrdin, Z. R. Ismagilov, E. S. Mikhailova, T. V. Rodionova, G. V. Villevald, and V. Y. Malysheva, 2018, The formation of carbon dioxide hydrate from water sorbed by coals: Fuel, **228**, 123–131, doi: 10.1016/j.fuel.2018.04.131.
Smirnov, V. G., A. Y. Manakov, E. A. Ukraintseva, G. V. Villevald, T. D. Karpova, V. V. Dyrdin, S. Yu. Lyrshchikov, Z. R. Ismagilov, I. S. Terekhova, and A. G. Ogienko, 2016, Formation and decomposition of methane hydrate in coal: Fuel, **166**, 188–195, doi: 10.1016/j.fuel.2015.10.123.
Waite, W. F., J. C. Santamarina, D. D. Cortes, B. Dugan, D. N. Espinoza, J. Germaine, J. Jang, J. W. Jung, T. J. Kneafsey, H. Shin, K. Soga, W. J. Winters, and T.-S. Yun, 2009, Physical properties of hydrate-bearing sediments: Reviews of Geophysics, **47**, RG4003, doi: 10.1029/2008RG000279.
Winters, W. J., W. P. Dillon, I. A. Pecher, and D. H. Mason, 2000, GHASTLI — Determining physical properties of sediment containing natural and laboratory-formed gas hydrate (Chapter 24), *in* M. D. Max, ed., Natural gas hydrate. Coastal systems and continental margins: Springer, **5**, 311–322.
Yang, L., A. Falenty, M. Chaouachi, D. Haberthür, and W. F. Kuhs, 2016, Synchrotron X-ray computed microtomography study on gas hydrate decomposition in a sedimentary matrix: Geochemistry, Geophysics, Geosystems, **17**, 3717–3732, doi: 10.1002/2016GC006521.
Zeng, Q., Z. Wang, B. J. McPherson, and J. D. McLennan, 2017, Modeling competitive adsorption between methane and water on coals: Energy & Fuels, **31**, 10775–10786, doi: 10.1021/acs.energyfuels.7b01931.

Biographies and photographs of the authors are not available.